Am J Physiol Endocrinol Metab 323: E492–E502, 2022.
First published October 12, 2022; doi:10.1152/ajpendo.00123.2022

american physiological society

AMERICAN JOURNAL OF PHYSIOLOGY
ENDOCRINOLOGY AND METABOLISM

RESEARCH ARTICLE

Coordination of pancreatic islet rhythmic activity by delayed negative feedback

N. Bruce,[1]* I.-A. Wei,[2]* W. Leng,[2] Y. Oh,[1] Y.-C. Chiu,[3] M. G. Roper,[2] and R. Bertram[1,4]

[1]*Department of Mathematics, Florida State University, Tallahassee, Florida;* [2]*Department of Chemistry and Biochemistry, Florida State University, Tallahassee, Florida;* [3]*Department of Physics, Florida State University, Tallahassee, Florida; and* [4]*Programs in Molecular Biophysics and Neuroscience, Florida State University, Tallahassee, Florida*

Abstract

Secretion of insulin from the pancreas is pulsatile, driven by intrinsic oscillations within individual islets of Langerhans. The secretions are coordinated among the many islets distributed throughout the pancreas producing a synchronized rhythm in vivo that is essential for maintaining normal glucose levels. One hypothesized mechanism for the coordination of islet activity is negative feedback, whereby sequestration of glucose in response to elevated insulin leads to a reduction in the blood glucose level that is sensed by the islet population. This global signal of glucose then coordinates the individual islets. In this study, we tested how this coordination mechanism is affected by time delays in the negative feedback, using a microfluidic system to monitor Ca^{2+} levels in a small population of islets and implementing glucose control through a negative feedback system. We found that islet synchronization occurs even with time delays in the feedback of up to 7 min. We also found that a second, slower closed-loop oscillation period is produced during delayed feedback in which islet oscillations are clustered into episodes. The period of this second oscillatory mode increases with the time delay and appears to be a second stable behavior that coexists with the faster synchronized oscillation. The general conclusion is that islet coordination through negative feedback is a viable means of islet coordination that is robust to delays in the timing of the feedback, and could complement other potential coordination mechanisms such as entrainment by pancreatic ganglia.

NEW & NOTEWORTHY Insulin secretion from islets of Langerhans is rhythmic, and these rhythms are coordinated to produce oscillatory plasma insulin levels. Using a combination of microfluidics and computational modeling, we demonstrate that coordination can occur through negative feedback of the type provided by the liver, even if that feedback is delayed by several minutes. We also demonstrate that a second, slower, mode of oscillations can occur when feedback is delayed where faster oscillations are grouped into episodes.

bistability; insulin; microfluidics; oscillations; synchronization

INTRODUCTION

Insulin is secreted by β-cells located within pancreatic islets of Langerhans in response to elevations in the blood glucose level. The hormone acts on downstream targets to facilitate glucose uptake and metabolism, and the storage of glucose in the form of glycogen in liver hepatocytes. The net result is a reduction of the blood glucose level and a subsequent reduction in insulin secretion. Thus, there is a whole body negative feedback loop involving insulin secretion that is key to glucose homeostasis. As with any such feedback loop, its effectiveness is determined largely by the speed of the feedback process. Fast negative feedback promotes homeostasis, whereas slow negative feedback promotes oscillations (1). An example of fast negative feedback is the voltage clamp technique that has been used in single-cell electrophysiology studies for decades (2). Here, the membrane potential of a cell is clamped by injecting current through an electrode that opposes any depolarizations or hyperpolarizations that would occur through the action of intrinsic ion channels. Because the negative feedback is very fast, the membrane potential remains nearly constant (homeostasis). An example of slow negative feedback is the *period* gene system for circadian oscillations. The *period* gene is transcribed and translated into PERIOD protein, which after heterodimerization and post-translational modifications, enters the nucleus and acts as a repressor of *period* gene transcription. Because this negative feedback process is slow, the PERIOD protein levels oscillate approximately every 24 h (3, 4). In the current study, we examine the effects of delayed negative feedback on the coordination of islet activity, using a combination of mathematical modeling and in vitro experimentation.

Single islets exhibit oscillatory activity, due to bursts of electrical impulses and accompanying oscillations in the intracellular Ca^{2+} concentration ($[Ca^{2+}]_i$) reflecting Ca^{2+} entry with each burst (5, 6). The $[Ca^{2+}]_i$ oscillations evoke pulsatile insulin secretion (5, 7). In the intact animal, blood insulin has this same pulsatility (8–11), indicating that the

*N. Bruce and I.-A. Wei contributed equally to this work.
Correspondence: R. Bertram (rbertram@fsu.edu).
Submitted 24 May 2022 / Revised 4 October 2022 / Accepted 8 October 2022

pulses of insulin from the thousands (rodents) or millions (humans) of islets within a pancreas are substantially coordinated. Pulsatile insulin release is essential for effective hepatic insulin action (12) and perturbations of pulsatile insulin secretion are observed in type II diabetics (7, 13).

Two coordination mechanisms have been proposed for islets (14). In one mechanism, an enteric nervous system within the pancreas provides neural input to islets that coordinates their oscillations. Support for this comes from findings of rich innervation of the pancreas by preganglionic vagal neurons that in some cases are coincident with islets (15, 16) and by recordings of bursts of electrical activity in ganglion cells that occur every 6–8 min (17). We have demonstrated that this neural forcing mechanism can lead to islet synchronization even if the forcing is aperiodic (18). A second mechanism postulates that coordination is achieved through feedback interactions between the pancreas and liver hepatocytes. In particular, the action of hepatocytes to lower blood glucose levels in response to insulin, providing negative feedback on insulin secretion, is the key to the coordination since all islets sense the same glucose level thereby acting as a global coordinating signal (14, 19). We have also tested the feasibility of this mechanism in an in vitro setting, and showed that it is effective at synchronizing islets so that pulses of $[Ca^{2+}]_i$ occur together throughout a small islet population (20).

In this report, we examine how the introduction of a time delay into the negative feedback affects the ability to achieve the coordination of islet activity. This question is motivated by the inherent time required for glycogen production in the liver, and for blood circulation through the body and into pancreatic capillaries where changes in the glucose level produced by the liver would be sensed by islets. We take two parallel approaches for this examination. In one, mathematical modeling is used with a population of islets coupled to a negative feedback system that regulates the glucose concentration based on a variable reflecting insulin concentration, as was done previously (19). An explicit time delay is now introduced so that the glucose response is delayed relative to the insulin level by an amount that is set by a delay parameter. The second approach is to monitor $[Ca^{2+}]_i$ as a proxy for insulin secretion from murine islets and adjust the glucose level delivered to the islets in response. A high $[Ca^{2+}]_i$ causes a reduced glucose level and vice versa, and the two variables of glucose and $[Ca^{2+}]_i$ change dynamically over time (20). As in model simulations, an explicit time delay is built into this negative feedback system, and its effect on islet coordination is determined.

Computer simulations with model islets demonstrate that even with time delays of several minutes, negative feedback is capable of coordinating islet activity. Furthermore, two types of rhythmic behavior can be achieved. In one, the period of the closed-loop system is similar to the natural periods of the uncoupled islets, regardless of the delay time, and pulses of islet activity are largely synchronized. We refer to these as "fast closed-loop oscillations" with periods near 5 min. In the other case, the closed-loop system exhibits a slower oscillation that increases linearly with the delay time. These so-called "slow closed-loop oscillations" indicate that the delayed negative feedback is intrinsically part of the rhythm generation, similar to the oscillations generated generically in a system with delayed negative feedback (1). That is, in this case, the delayed negative feedback does not synchronize the islets to oscillate together, but introduces a second rhythmic component that groups the faster oscillations into slower episodes. These model predictions are tested in vitro and shown to be generally valid. Thus, coordinated islet activity is achieved in both cases, with evidence for both fast and slow closed-loop oscillations. Overall, the study demonstrates, in a well-controlled in vitro setting, that negative feedback is a robust means for coordinating islet activity and can produce oscillations in the population that have significantly longer periods than the mean natural periods of the uncoupled islets.

MATERIALS AND METHODS

Chemicals and Reagents

Sodium chloride (NaCl), calcium chloride ($CaCl_2$), magnesium chloride ($MgCl_2$), dimethyl sulfoxide (DMSO), and Fura PE3 acetoxymethyl ester (AM) were acquired from Sigma-Aldrich (Saint Louis, MO). Potassium chloride (KCl) and tricine were from VWR International (Radnor, PA). Sodium hydroxide (NaOH), glucose (dextrose), and bovine serum albumin (BSA) were purchased from Fisher Scientific (Pittsburgh, PA). Fetal bovine serum (FBS), penicillin-streptomycin, gentamicin, and Pluronic F-127 were from Thermo Fisher Scientific (Waltham, MA). Collagenase P was from Roche Diagnostics (Indianapolis, IN). RPMI 1640 was from Corning (Corning, NY). Polydimethylsiloxane (PDMS) and curing agent were from Dow Corning (Midland, MI). SU-8 photoresist was from Kayaku Advanced Materials (Westborough, MA). All solutions were made with ultrapure deionized (DI) water (Millipore, Bedford, MA). Glucose solutions were prepared in a balanced salt solution (BSS) composed of 125 mM NaCl, 5.9 mM KCl, 2.4 mM $CaCl_2$, 1.2 mM $MgCl_2$, and 25 mM tricine, at pH 7.4, with 1 $mg{\cdot}mL^{-1}$ BSA.

Isolation and Culture of Islets of Langerhans

The islet isolation protocol was approved by the Florida State University Animal Care and Use Committee (Protocol No. 202000078). Islets of Langerhans were obtained from 25–40 g male CD-1 mice (Charles River Laboratories, Wilmington, MA) by collagenase P digestion as described previously (21, 22). Isolated islets were incubated in RPMI 1640 medium with 11 mM glucose, L-glutamine, 10% FBS, 100 $U{\cdot}mL^{-1}$ penicillin, 100 $\mu g{\cdot}mL^{-1}$ streptomycin, and 10 $\mu g{\cdot}mL^{-1}$ gentamicin at 37°C and 5% CO_2. Islets were kept in the incubator and used within 4 days after isolation. Typically, islets were isolated from two mice and mixed during experiments.

Microfluidic Device and $[Ca^{2+}]_i$ Detection

A PDMS-glass hybrid device was adopted from previous work (20). The device was fabricated using soft lithography with SU-8 2075 photoresist. All channels were 250 × 40 μm (width × height). The device had two inputs, each connected to a 60-mL syringe filled with 10 mL of BSS containing 3 and 13 mM glucose, respectively. The relative heights of these two syringes were controlled with a stepper motor and pulley system using a LabVIEW program (National Instruments,

Austin, TX) (23). This system produced different flow rate ratios of the glucose solutions into the device without changing the total flow rate delivered to the islet chamber. The two solutions mixed and produced a final glucose concentration perfused into the 0.6-mm diameter islet chamber (Fig. 1*A*) The final concentration delivered to the islet chamber was calibrated to the heights of the syringes as described previously (22, 23). The time for a new glucose concentration to be delivered to the islet chamber was 24 ± 1 s (n = 3). The temperature of the islet chamber was maintained at a temperature of 36 ± 0.5°C using a thermofoil heater, thermocouple, and control system as described elsewhere (18).

To measure $[Ca^{2+}]_i$, 1 μL of 5 mM Fura PE3 AM in DMSO and 1 μL of Pluronic F-127 in DMSO were added to 1.998 mL of RPMI 1640 medium. Islets were incubated in this solution at 37°C and 5% CO_2 for 40 min. After incubation, islets were removed, rinsed in a dish containing BSS with 10 mM glucose, and loaded manually into the microfluidic device that had been filled with BSS containing 10 mM glucose. Islets were allowed to equilibrate to the perfusion flow for 5 min before recording.

The widefield epifluorescence $[Ca^{2+}]_i$ imaging system is similar as previously described (26). A xenon arc lamp with a filter wheel and shutter (Sutter Instruments, Novato, CA) was used for excitation of Fura PE3 within islets using 340 ± 5 and 380 ± 5 nm filters (Omega Optical 340AF15 and 380AF15, Brattleboro, VT). Collimated excitation light was made incident on a 409 nm dichroic mirror (Thorlabs, Inc., Newton, NJ) that was then focused onto the sample using a ×10, 0.5 numerical aperture (NA) objective (Nikon Instruments, Melville, NY). Emission was collected by the same objective, passed through the dichroic mirror and through a 510 nm ± 84 nm emission filter (Semrock, Rochester, NY) before detection by a CCD camera (QImaging, Surrey, BC, Canada). Image acquisition was 150 ms for each excitation wavelength every 20 s. The ratio of fluorescence intensity after excitation at 340 and 380 nm was collected to calculate the free $[Ca^{2+}]_i$ within each islet using calibration values determined by previously reported methods (27).

In Vitro Closed-Loop Glucose Control

When in the closed-loop configuration, the extracellular glucose concentration (G_e) was controlled as described in Ref. 20. The free $[Ca^{2+}]_i$ from each islet was averaged across all islets, Ca_{avg}, and converted to a measure of average insulin secretion in arbitrary units, I_{avg}, using *Eq. 1*. This is an increasing linear function of Ca_{avg} past a threshold value, Ca_{thr}:

$$I_{avg} = \begin{cases} I_{slope}(Ca_{avg} - Ca_{thr}) & \text{for } Ca_{avg} \geq Ca_{thr} \\ 0 & \text{for } Ca_{avg} < Ca_{thr} \end{cases}, \quad (1)$$

Ca_{thr} was determined by:

$$Ca_{thr} = (Ca_{max} - Ca_{min})\kappa + Ca_{min}, \quad (2)$$

where Ca_{max} and Ca_{min} are the maximum and minimum of the Ca_{avg} from all islets, respectively, dependent on the individual experiment, and κ is a parameter (Table 1). G_e was updated using the following differential equation:

$$\frac{dG_e}{dt} = \frac{G_\infty - G_e}{\tau_G}. \quad (3)$$

The parameter τ_G is a time constant for the feedback response and the asymptotic extracellular glucose response function, G_∞, is a decreasing sigmoidal function of I_{avg} with a time delay of τ_d:

$$G_\infty = G_{min} + \frac{G_{max} - G_{min}}{1 + \exp\left(\frac{I_{avg}(t-\tau_d) - \hat{I}}{S_G}\right)}, \quad (4)$$

$\hat{I}$ corresponds to the inflection point halfway between the minimum and maximum glucose levels, G_{min} and

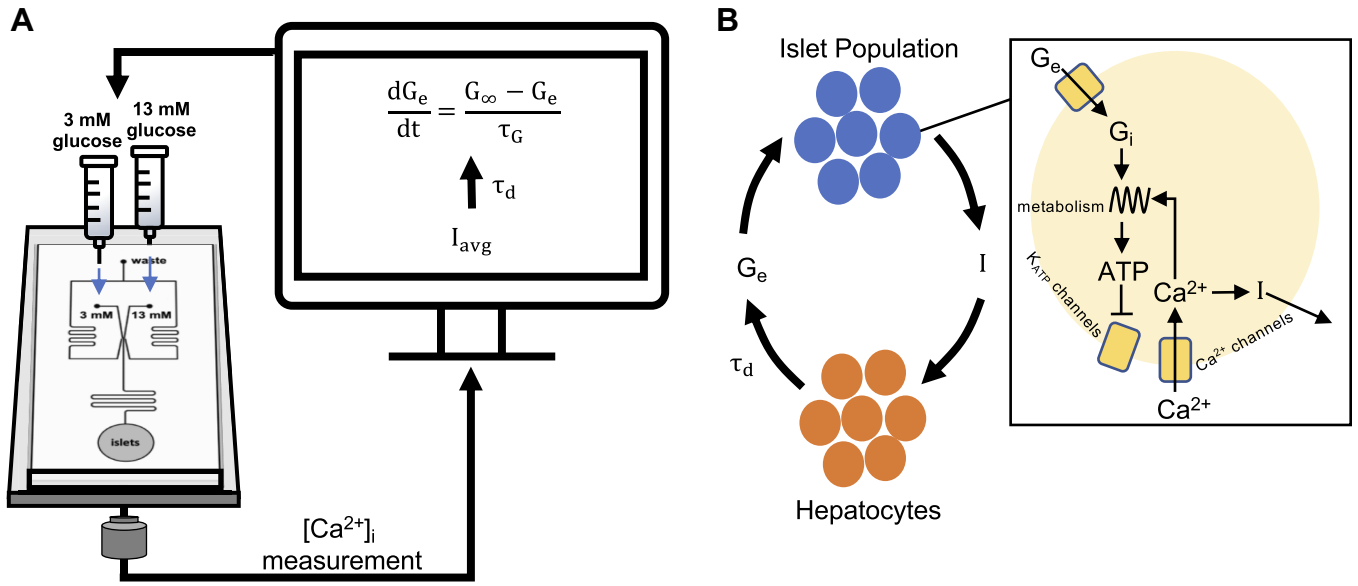

Figure 1. Closed-loop feedback system. *A*: beginning from the left, a microfluidic device delivers varying glucose concentrations to a population of 3–6 islets and $[Ca^{2+}]_i$ from each islet is measured. The average $[Ca^{2+}]_i$ of the population is converted to an average insulin measurement (I_{avg}) using an increasing linear relationship. I_{avg} is input into a glucose response function (G_∞), which is a decreasing sigmoidal function of insulin with an explicit time delay (τ_d). G_∞ is used to update the extracellular glucose concentration (G_e) that is delivered to the islets to close the loop. *B*: diagram of the negative feedback loop with the Integrated Oscillator Model (IOM). G_e, extracellular glucose. G_i, intracellular glucose. I, insulin; τ_d, time delay.

Table 1. *Experimental parameters*

I_{slope} = 1 nM^{-1}	κ = 0.1	Ca_{max} = varied (nM)	Ca_{min} = varied (nM)
G_{min} = 7 mM	G_{max} = 13 mM	τ_d = varied (min)	$\hat{I}$ = varied
τ_G = 50,000 ms	S_G = 1		

G_{max}, respectively, and was dependent on the experiment. The parameter S_G determines the steepness of the response (Table 1).

The differential equation was discretized using the forward Euler method with a 1-s time step. The values for Ca_{avg} and I_{avg} were updated every 20 time steps, since Ca^{2+} measurements are made each 20 s. All parameters are given in Table 1. The key parameter varied to investigate the synchronization capabilities of the feedback was the time delay, τ_d, between the experimental measurement of Ca_{avg} and the change in G_e (this added time delay is in addition to the time required for changes in glucose concentration to reach the islets). In the experiments, τ_d values of 0, 3, 6, and 7 min were used.

Mathematical Model of Islet Oscillations

The mathematical model of islet activity is based on the Integrated Oscillator Model (IOM) (28, 29), which describes a system in which metabolic and electrical oscillations are produced. This model consists of eight differential equations for membrane potential, activation of a delayed rectifying K^+ current, the concentrations of metabolites fructose 6-phosphate (F6P), fructose 1,6-bisphosphate (FBP), adenosine diphosphate (ADP), and the concentrations of free Ca^{2+} in the cytoplasm, endoplasmic reticulum (ER), and mitochondria. The metabolic and electrical interactions are bidirectional. ATP produced through glucose metabolism affects the electrical oscillator by closing K^+ channels, thus depolarizing the plasma membrane. The subsequent influx of Ca^{2+} into the cytoplasm then affects metabolism by activating dehydrogenases and electrical effects of crossing the mitochondrial inner membrane (30, 31). The IOM is able to replicate diverse oscillations in metabolism, electrical activity, and $[Ca^{2+}]_i$ that have been observed experimentally (29, 32–34). Cells within an islet are coordinated through gap junctions, motivating our modeling approach in which a single cell reflects the behavior of all β-cells within an islet. Although the significant heterogeneity among β-cells and behaviors such as Ca^{2+} waves are important features on a shorter timescale of seconds (35–38), the approximation made by the IOM is appropriate for the time scale of minutes that is our focus.

The IOM was modified to simulate negative feedback from target cells similar to what was done previously (19) and illustrated in Fig. 1*B*. First, the rate of insulin secretion for each islet is described by

$$\frac{dI}{dt} = \frac{I_\infty - I}{\tau_I}, \tag{5}$$

where τ_I is a time constant and the equilibrium secretion rate, I_∞ is an increasing linear function of the Ca^{2+} concentration (Ca), past a threshold value, Ca_{thr}:

$$I_\infty = \begin{cases} I_{slope}(Ca - Ca_{thr}) & \text{for } Ca \geq Ca_{thr} \\ 0 & \text{for } Ca < Ca_{thr} \end{cases}. \tag{6}$$

The equation for intracellular glucose concentration (G_i) for each islet is given by:

$$\frac{dG_i}{dt} = J_{glut} - J_{gk}. \tag{7}$$

The value J_{glut} is the GLUT-2 facilitated glucose transporter flux:

$$J_{glut} = V_{glut}\frac{(G_e - G_i)K_{glut}}{(K_{glut} + G_e)(K_{glut} + G_i)}, \tag{8}$$

where V_{glut} is the maximal rate and K_{glut} is a shape parameter. The glucokinase reaction flux, J_{gk}, is an increasing Hill function of G_i:

$$J_{gk} = V_{gk}\frac{G_i^{n_{gk}}}{K_{gk}^{n_{gk}} + G_i^{n_{gk}}}. \tag{9}$$

The parameter V_{gk} is a glucose sensitivity parameter and is varied between the model islets to create a heterogeneous islet population. This parameter has a strong effect on the islet oscillation period (as was also the case in a different β-cell model, shown in Ref. 38), and values were chosen to give single-islet oscillation periods of several minutes that were similar to those of the biological islets used in our experiments. If different parameters are used to generate a heterogeneous islet population, all results of the study are replicated.

The insulin secretion is averaged among all islets to give I_{avg}. The equation for extracellular glucose concentration (G_e) is the same as *Eq. 3* in the experimental feedback system with *Eq. 4* as the glucose response function. The parameters for the model are shown in Table 2. In the model, τ_d values of 0, 1, 2, 3, 4, 5, 6, and 7 min were used.

Data Analysis

The natural period of individual islets was calculated by averaging the time between peaks of $[Ca^{2+}]_i$ before feedback began. The oscillation period of Ca_{avg} after feedback was calculated using spectral analysis. Specifically, the frequency spectrum was found using a Fast Fourier Transform (FFT) of the Ca_{avg} signal once the feedback loop was closed. The inverse of the peak of the frequency spectrum was taken to be the synchronized oscillation period, with any secondary peak, if present, taken to be the secondary oscillation period.

RESULTS

We have previously shown that negative feedback without a time delay can synchronize islet populations. These experiments were performed using a microfluidic system to deliver glucose to islets, the average $[Ca^{2+}]_i$ in response was measured, and a new glucose level was delivered in response. In

Table 2. *Model parameters*

τ_I = 10,000 ms	V_{glut} = 8 mM·ms^{-1}	K_{gk} = 11 mM	τ_d = varied (min)
I_{slope} = 1,000 μM^{-1}	K_{glut} = 7 mM	G_{min} = 7 mM	$\hat{I}$ = 15
Ca_{thr} = 0.1 μM	V_{gk} = varied (mM·ms^{-1})	G_{max} = 13 mM	S_G = 1
τ_G = 50,000 ms	n_{gk} = 15		

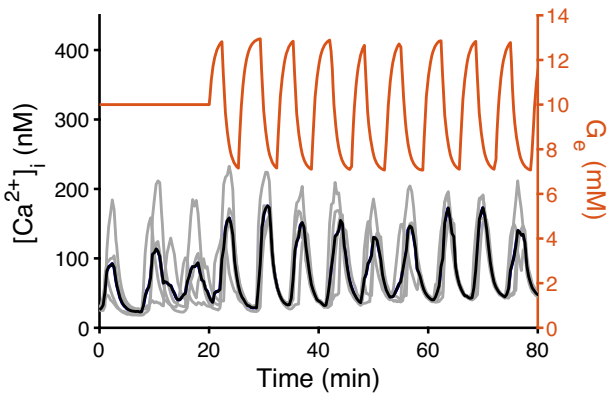

Figure 2. Islets synchronized in the closed-loop system without time delay. Gray lines represent individual $[Ca^{2+}]_i$ traces for four islets, the black line represents average Ca_{avg} and the orange line represents extracellular glucose concentration (G_e). During the initial delivery of a constant 10 mM glucose, islets oscillated out of phase with different periods, resulting in low amplitude Ca_{avg} oscillations. When the feedback was turned on after 20 min, the individual islet oscillations synchronized to a 6-min period, resulting in larger, more regular Ca_{avg} oscillations.

this previous system, time delays were not considered. Here, we use both modeling and experiments to explore how time delays in the feedback loop affect the coordination of islet populations (Fig. 1).

Islets Synchronize with Negative Feedback and No Time Delay

Initial experiments set out to reproduce the previous measurements that demonstrated islets can be synchronized without a time delay (τ_d = 0) in the feedback loop (20). As shown in Fig. 2, a constant glucose concentration of 10 mM was delivered to groups of 3–6 islets. During this time, the islets exhibited oscillatory activity, as seen through measurements of $[Ca^{2+}]_i$ (gray curves); however, these oscillations were not in phase since the islets were uncoupled. The natural period of each islet varied over the range 3–10 min. After 20 min, feedback was turned on with no added time delay, forming a closed-loop by delivering a new G_e in response to Ca_{avg}, as done previously (20), resulting in a synchronization of the $[Ca^{2+}]_i$ oscillations. As a result of the synchronization, the regularity and amplitude of the Ca_{avg} oscillations increased once the loop was closed.

Once the feedback was activated at 20 min, glucose oscillations were immediately established (Fig. 2). It is evident that the oscillations in G_e and Ca_{avg} are ~180° out of phase; that is, the peak in Ca_{avg} corresponds to the nadir of G_e. In this case, the period of the closed-loop system (6.7 min) was within the range of the natural oscillation periods of the individual islets (5.9, 7.3, 8.3, and 10.3 min before feedback), and is an example of "fast closed-loop oscillations."

Model Islets Produce Fast Closed-Loop Oscillations with and without a Time Delay

In parallel with the in vitro experiments, a mathematical model of islets was used to predict possible coordination properties due to the negative feedback, with and without a time delay. When there was no time delay (τ_d = 0 min), five model islets synchronized rapidly once the feedback loop was closed (Fig. 3*A*). Before activation of the feedback, the model islets exhibited slow bursting with oscillation periods of 9.4, 7.5, 5.3, 4.7, and 4.5 min. Once the loop was closed, all islets oscillated in phase with one another for a period of 4.2 min, indicating that fast closed-loop oscillations occurred.

Model islets also synchronized when a time delay was used in the feedback loop. Synchronization of model islets with a 3, 6, and 7 min time delay (τ_d = 3, 6, 7 min) is shown in Fig. 3, *B–D*, respectively. The closed-loop oscillation period of Ca_{avg} in each case was close to 4 min, similar to what was

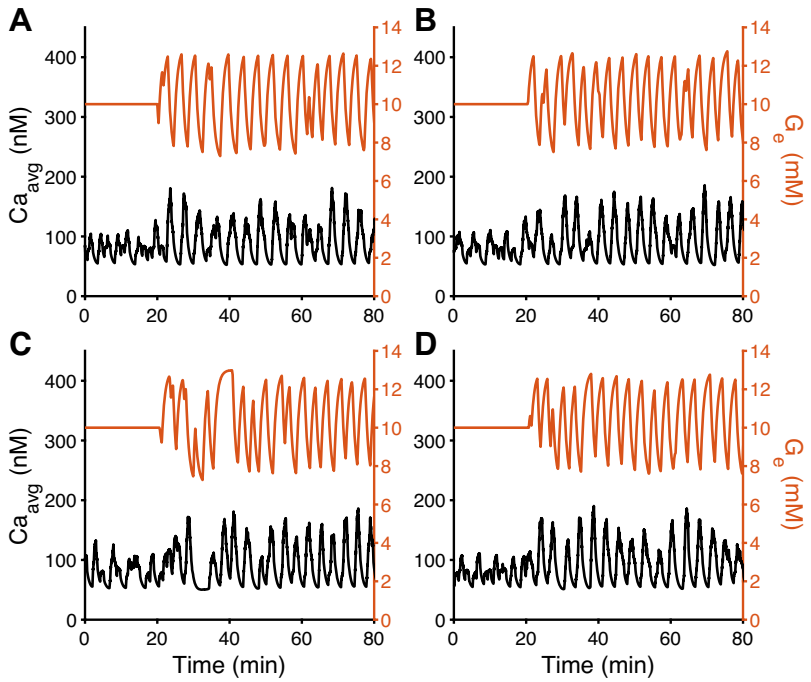

Figure 3. Model islets synchronize with and without a time delay to produce a fast oscillation in Ca_{avg}. Five model islets were simulated with natural periods ranging between 4 and 10 min by varying the glucose sensitivity parameter V_{gk} between 0.0015 and 0.0029 $\mu M \cdot ms^{-1}$ among the islets. Feedback was turned on after 20 min. The parameter values are the same in each panel, except for the delay τ_d. *A*: feedback with τ_d = 0 min synchronized islets to a 4.2-min period. *B*: feedback with τ_d = 3 min synchronized islets to a 3.6-min period. *C*: feedback with τ_d = 6 min synchronized islets to a 3.8-min period. *D*: feedback with τ_d = 7 min synchronized islets to a 4.0-min period.

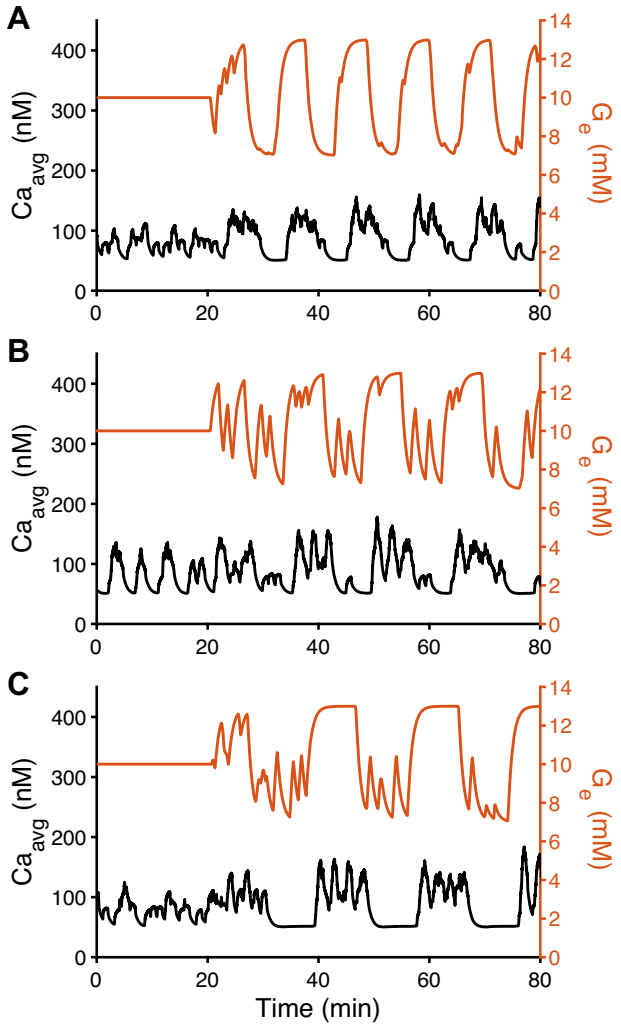

Figure 4. Negative feedback can coordinate islets to produce a slow oscillation in Ca_{avg} when there is a time delay. In each of the simulations, the parameter values of the model islets were the same as in Fig. 3. only the initial conditions were different. However, in these cases, slow closed-loop oscillations were observed with a period of 11.5 min with τ_d = 3 min (*A*), with a 15.3-min period with τ_d = 6 min (*B*), and with a 19.6-min period with τ_d = 7 min (*C*).

observed for τ_d = 0 min. Thus, the model predicts that fast closed-loop oscillations can occur both with and without a time delay.

With a Delay, Slow Closed-Loop Oscillations Can Be Achieved in Model Islets

Synchronization of model islets was not the only behavior observed in model simulations. In addition to synchronization to a fast oscillation period, feedback with a time delay also produced oscillations in Ca_{avg} with a longer period. Examples of this for τ_d = 3, 6, 7 min are shown in Fig. 4. The model islets had parameter values identical to those used in Fig. 3, yielding the same natural periods of 9.4, 7.5, 5.3, 4.7, and 4.5 min before feedback. In contrast to what was observed previously, for each time delay value, the closed-loop oscillation period (11.5 min, 15.3 min, and 19.6 min) was considerably longer than the natural periods of the model islets.

The individual islet activity for fast and slow oscillations in the presence of delayed feedback is shown in Fig. 5. For τ_d = 3 min, the fast oscillations in Ca_{avg} observed in Fig. 3*B* are the result of individual model islets synchronizing to a fast oscillation period (Fig. 5*A*). There is a small amount of drift in the traces that is indicative of an additional slow oscillation mode since the drift appears to be periodic. However, the effect is small and is not reflected in the average trace, which exhibits a fast 3.6 min period. The slow oscillations in Ca_{avg} observed in Fig. 4*A* are the result of model islets oscillating individually with fast periods that are clustered together into slow episodes (Fig. 5*B*). Thus, the individual islet oscillations persisted, but were not synchronized as each islet oscillated out of phase and in an independent pattern with respect to the other islets. Instead, the oscillations became grouped into episodes that occurred much less frequently than the individual islet oscillations.

Biological Islets Also Have Closed-Loop Oscillations with Long Periods

The modeling results from Figs. 3, 4, and 5 make the predictions that heterogeneous islet oscillators can become coordinated even if there is a delay in the feedback and that there are two distinct types of closed-loop oscillations: fast and slow. These results were tested by delivering glucose levels to murine islets held in a microfluidic device. In one example using a 3-min time delay (τ_d = 3 min) with a population of five

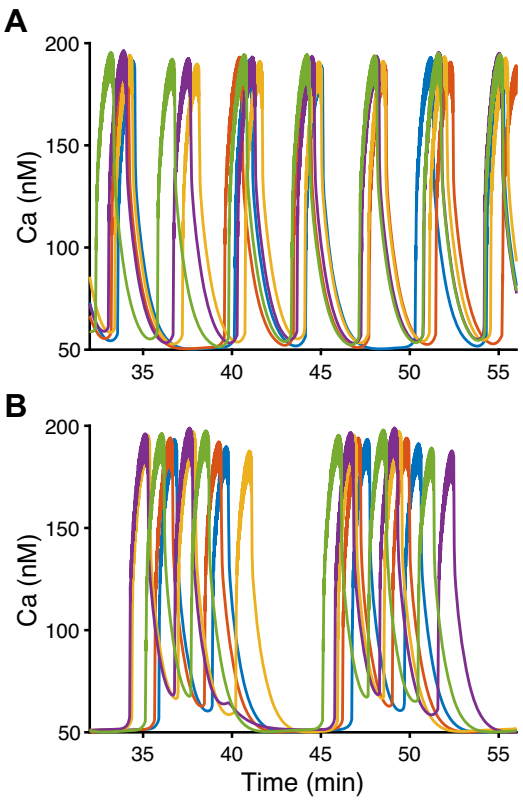

Figure 5. Individual traces during fast and slow oscillations in the presence of delayed feedback. *A*: feedback with τ_d = 3 min synchronized model islets to a fast 3.6-min period with islets oscillating roughly in phase with one another. *B*: feedback with τ_d = 3 min grouped model islets into episodes with a slow 11.5-min period.

islets, the islets synchronized to a fast 3.6-min oscillation period (Fig. 6*A*), demonstrating that time delays do not necessarily interfere with synchronized oscillations. In contrast, using the same condition, another population of five islets exhibited a slow 10.2-min oscillation period (Fig. 6*B*). The individual islet activity for the slow oscillations is similar to what was seen in model islets, with the fast oscillations grouped into slow episodes (Fig. 7*A*). A 6-min time delay resulted in islets exhibiting a faster closed-loop oscillation with 5.5-min period (Fig. 6*C*). There is a slower oscillation pattern in the Ca_{avg} amplitude that is also present in the individual islet oscillations (Fig. 7*B*). This was further analyzed through spectral analysis, which revealed a major mode at 5.5-min period and a weaker mode (the second largest peak in the spectrum) at 15.1 min. This slower oscillation is better revealed using moving averages for G_e and Ca_{avg}, with a time window of 6 min (green curves in Fig. 6*C*). Finally, even with a 7-min time delay, another population of six islets exhibited a fast closed-loop oscillation of 3.7 min (Fig. 6*D*).

The Response to Delayed Negative Feedback Exhibits Bistability

The periods of both fast and slow closed-loop oscillations in model islets are quantified in Fig. 8*A*. The lower set of points corresponds to the fast closed-loop oscillations, with periods near 4 min for all delay values. There is also a separate branch of points corresponding to the slow closed-loop oscillations that were obtained using a different set of initial conditions than those used for the fast closed-loop oscillations. For these slow closed-loop oscillations, the period increased linearly with the time delay, as shown with the regression line (slope $m = 2.1$, $R^2 = 0.97$).

To determine whether a similar pattern of closed-loop oscillations occurred in the in vitro experiments, the resulting oscillation periods at different time delays (0, 3, 6, and 7 min) were quantified and shown in Fig. 8*B*. Only fast closed-loop oscillations were observed in the three sets of islets examined without a time delay ($\tau_d = 0$ min). Both fast and slow oscillations were produced for $\tau_d = 3$ min, though for one case, the slow component was secondary to the fast component in the power spectrum (red point). In the case of $\tau_d = 6$ min, which was performed on four sets of islets, closed-loop oscillations were fast or had fast dominant modes. However, in two cases there were secondary components in the power spectrum with a period of ~15.1 min (red points), such as shown in Fig. 6*C*. In the two experiments performed with $\tau_d = 7$ min, the closed-loop oscillations were fast. These results are consistent with the model prediction of two sets of closed-loop oscillations, with the period of the fast oscillations independent of the delay time and that of the slow closed-loop oscillations increasing linearly with the delay time (regression line slope $m = 1.7$, $R^2 = 0.98$).

Figure 8 demonstrates that often for the same time delay, islets are either synchronized in a fast oscillation or clustered into episodes in a slow oscillation. One explanation for this is that the islet properties are different in the different cases; some islet properties are such that fast closed-loop oscillations will occur whereas others facilitate slow closed-loop oscillations. Yet, in our model islets, we found that the same model islets were capable of producing both types of closed-loop oscillations. If the model islets were started with one set of initial conditions, fast closed-loop oscillations occurred, while if started from another set of initial conditions, slow closed-loop oscillations occurred. That is, the model closed-loop system is bistable.

To determine if biological islets also display bistability in a closed-loop system, we used a protocol in which G_e was initially clamped at 10 mM, allowed to vary in the closed-loop system, then clamped a second time at 10 mM, and finally allowed to vary once again. The rationale behind the second clamp was to allow the islets to drift

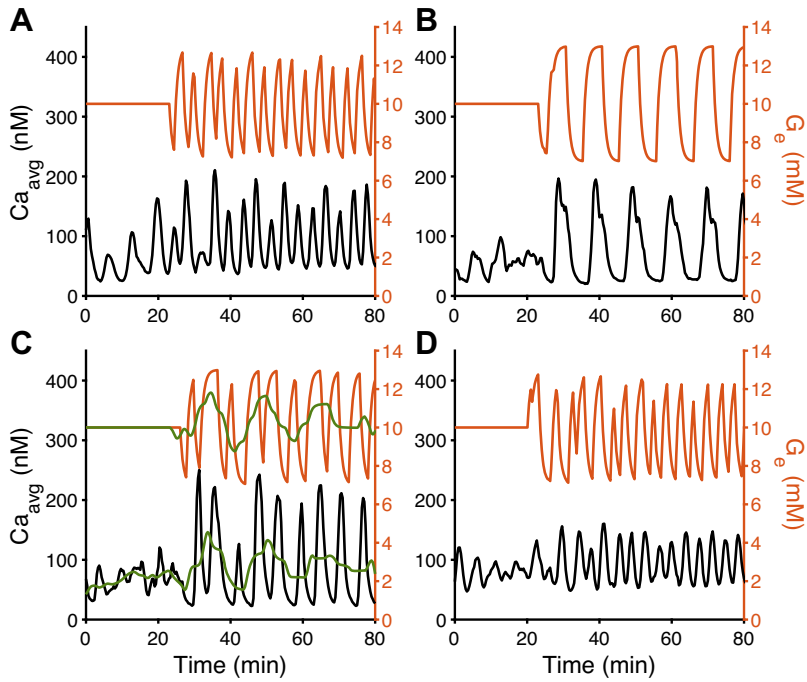

Figure 6. Murine islet oscillations are coordinated to produce either fast or slow closed-loop oscillations when the feedback is delayed. *A*: a delay of 3 min produces oscillations in Ca_{avg} with a period of 3.6 min in a population of five islets. *B*: a delay of 3 min on a different population of five islets leads to Ca_{avg} oscillations with a 10.2-min period. *C*: a delay of 6 min yields a fast oscillation in Ca_{avg} in a different population of six islets with primary period of 6 min. There is a secondary oscillation mode that is revealed using a moving average (green curve). *D*: a delay of 7 min yields a fast oscillation with a 3.7-min period in a different set of six islets.

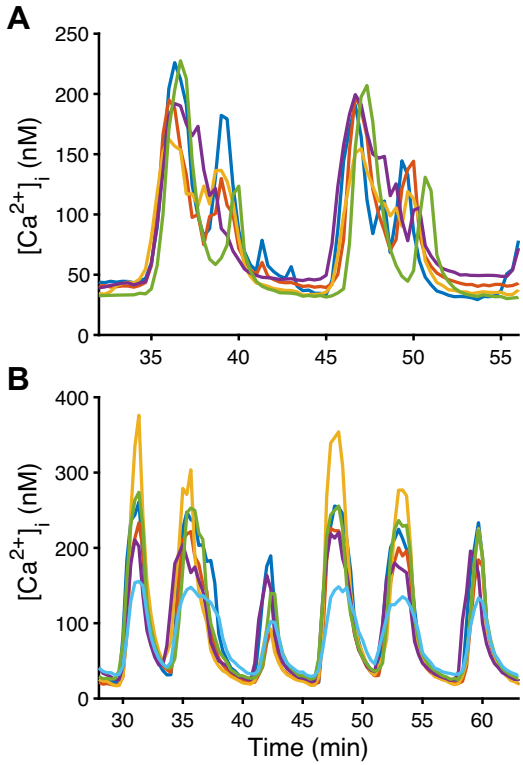

Figure 7. Individual traces of murine islets with a slow oscillation component in the presence of delayed negative feedback. *A*: feedback with τ_d = 3 min grouped islets into episodes with a slow 10.2-min period. *B*: feedback with τ_d = 6 min synchronized islets into a 6-min period with a secondary, slow oscillation pattern of 15.1 min in the $[Ca^{2+}]_i$ amplitude.

away from the periodic cycle achieved during the closed-loop configuration. This would effectively reset the "initial conditions" for when the closed-loop configuration was reestablished, so that the islets could potentially move to the alternate oscillatory cycle (if one indeed exists).

When this double-clamping protocol was applied to a population of five heterogeneous model islets with τ_d = 3 min, the islets exhibited a slow oscillation in Ca_{avg} with a period of 11.4 min when the closed-loop configuration was established the first time (Fig. 9*A*). As expected, the slow oscillation was eliminated when the glucose level was clamped again at 10 mM and the individual islet oscillators drifted apart due to their heterogeneity. However, when the closed-loop configuration was reestablished, the model islets exhibited a fast synchronized oscillation period of 3.6 min. Thus, this protocol was successful in revealing both fast and slow closed-loop oscillations in the same set of model islets. The same protocol was applied to four murine islets (Fig. 9*B*) and the result was remarkably similar. When the system entered the closed-loop configuration the first time, slow oscillations in Ca_{avg} occurred with a period of 9.8 min, and these quickly dissipated when the glucose level was again clamped and the islets drifted apart. When the closed-loop configuration was reestablished, fast oscillations occurred with a period of 3.5 min. This demonstrates bistability in the closed-loop system in the murine islets, and occurred in one of 10 experiments with different sets of islets.

DISCUSSION

Using a combination of simulations with mathematical models and in vitro experiments with murine islets, we have shown that rhythmic islet activity can be coordinated through a negative feedback process that regulates glucose levels, even in the presence of time delays in the feedback. A similar time delay would be expected in a physiological setting in which the negative feedback is provided by hepatocytes of the liver and other target tissue and is relayed to pancreatic islets through the general circulation. The fact that negative feedback control of glucose levels can be an effective coordinating force even with time delays provides support for similar coordination in vivo, where islet coordination is apparent through measurements of insulin pulsatility in the blood (8–10, 39). This coordination mechanism may complement another potential mechanism involving an enteric pancreatic nervous system that can provide neural stimuli to islets through synaptic connections (15, 16, 40, 41).

Although the feedback system often synchronized oscillations in the model and biological islets, resulting in fast closed-loop oscillations, an alternate pattern of activity sometimes occurred in which the oscillations were grouped into episodes (Fig. 5). This activity resulted in a slower rhythm in Ca_{avg} that we refer to as slow closed-loop oscillations (Figs. 4 and 6). Unlike the fast oscillations, the oscillation period of the slower ones increases linearly with the time delay (Fig. 8). In model islets, this linear increase in slow closed-loop period continues for time delays beyond 7 min, but this has not been tested in the microfluidic system.

An unexpected finding was that with a time delay there is bistability in the closed-loop system. We found no evidence for this when there was no time delay, in either this study or a previous one (20). To test the validity of this model prediction, we designed a glucose protocol that could switch the system from one oscillatory state to the other, and indeed such a

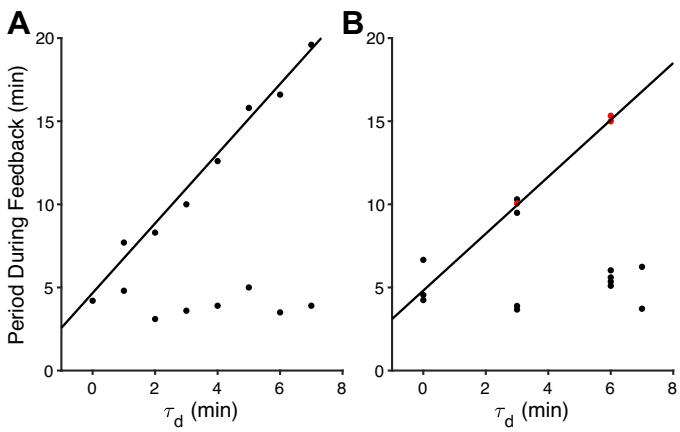

Figure 8. Closed-loop oscillation periods for different feedback delays. The oscillation periods during feedback (black points) are plotted for τ_d between 0 and 7 min. *A*: model oscillation periods indicate both fast and slow oscillations for each nonzero time delay. The relationship between slow oscillations and time delay fit a line with slope m = 2.1 and R^2 = 0.97 (black line). *B*: murine islet oscillation periods. The red points indicate a secondary peak in the power spectrum. The relationship between slow oscillations and time delay fit a line with slope m = 1.7 and R^2 = 0.98 (black line).

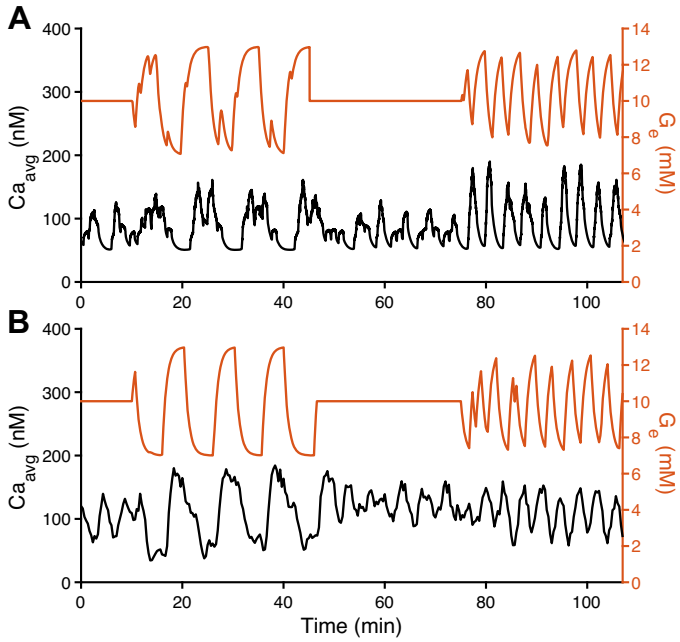

Figure 9. Bistability revealed in both model and biological islets using a double-clamp protocol. The system is in the closed-loop configuration with τ_d = 3 min from 10 to 45 min and from 75 to 110 min. *A*: five model islets exhibit slow oscillations with an 11.4-min period during the first closed-loop period, and fast oscillations with a 3.6-min period during the second. *B*: a population of four biological islets exhibit slow oscillations with a 9.8-min period during the first closed-loop period and switch to fast oscillations with a 3.5-min period during the second.

switch occurred in both model islets and in the biological islets (Fig. 9). The ability to switch from one attractor to the other through a perturbation of the system, as we have done, depends on the sizes of the basins of attraction of the two attractors; if the basin of attractor A is much larger than that of attractor B, then the likelihood of switching from A to B is low. Unfortunately, determining the size of a basin of attraction is very time consuming, even for mathematical models, and is impractical for experimental systems. In many model simulations, we could switch between fast and slow closed-loop oscillations ~10% of the time. It is therefore not surprising that we were able to achieve a switch from slow to fast closed-loop oscillations in only one of 10 attempts in the in vitro system.

There have been several reports of bistability in biological systems. These include elements of the cell cycle (42), tissue morphogenesis (43), the *lac* operon and lactose metabolism (44), electrically coupled networks of β cells (45), and a synthetically generated genetic toggle switch (46). In principle, all bistable systems can be switched from one attractor to the other, but the procedure most often used to identify bistability is the demonstration of hysteresis. That is, to slowly change a control parameter and establish that, over a range of parameter values, the asymptotic state is different when the parameter is increased than it is when the parameter is decreased through the same values (24). We know of fewer instances where the system has been reset from one attractor to the other as a demonstration of bistability, but one example seems relevant since it involves pancreatic islets. There is strong evidence that islet β-cells can exhibit intrinsic oscillations in glycolysis, which can drive bursting electrical activity through actions of adenine nucleotides on K(ATP) ion channels (29). A mathematical model suggests that there is a range of glucose levels over which the glycolytic subsystem is bistable between a stationary state and an oscillatory state. To test this prediction, islet electrical activity was monitored while the glucose level was reduced from a stimulatory level of 11.1 mM to 0 mM, and back to 11.1 mM. The response of the islet was to switch from a slow bursting mode to a continuous spiking mode; this was interpreted as a switch from active glycolytic oscillations to stationary glycolysis (25). This is perhaps parallel to what we see in Fig. 9; in both cases, the slow mode can act to group faster events into episodes (Fig. 5*B* and Fig. 7*A*) which in the case of the single islet study of Bertram et al. (25) was referred to as "compound bursting."

Our finding of islet synchronization through delayed negative feedback is restricted to the case of islet oscillations that have an intrinsic period on the order of several minutes or more (47–49). There are, however, many reports of much faster oscillations (period of 15–60 s) in islet Ca^{2+} or electrical activity (6, 47, 48, 50). In one study, it was found that islets examined from some mice are all fast, while islets examined from other mice are all slow (51). The physiological ramifications of these two phenotypes has not been examined. We focused on the slower ~5 min islet oscillators because this period is similar to the period of insulin oscillations that have been observed in peripheral and portal blood measurements (8–10). There are no data that we know of to indicate that fast islet oscillations, when they occur in vivo, are coordinated.

Conclusions

In conclusion, our results suggest that control of islet activity through a negative feedback system that acts through glucose is a viable means of coordinating islet activity and thereby producing coherent pulses of insulin secretion. We successfully tested it on a microfluidic system to interrogate the modulation of synchronized periods of islets using a delayed feedback system. The inclusion of time delays in the feedback system does not compromise the coordination, but it can introduce a second mode of slower rhythmicity.

GRANTS

This work was supported in part from National Institutes of Health under Grant Number R01 DK 080714 (to M.G.R.) and from the National Science Foundation under Grant Number DMS 1853342 (to R.B.).

DISCLOSURES

No conflicts of interest, financial or otherwise, are declared by the authors.

AUTHOR CONTRIBUTIONS

N.B., I.-A.W., W.L., Y.O., M.G.R., and R.B. conceived and designed research; I.-A.W. and W.L. performed experiments; N.B., I.-A.W., W.L., Y.O., Y.-C.C., M.G.R., and R.B. analyzed data; N.B., I.-A.W., W.L., Y.O., M.G.R., and R.B. interpreted results of experiments; N.B. and I.-A.W. prepared figures; N.B., I.-A.W., M.G.R., and R.B. drafted

manuscript; N.B., I.-A.W., M.G.R., and R.B. edited and revised manuscript; N.B., I.-A.W., W.L., Y.O., Y.-C.C., M.G.R., and R.B. approved final version of manuscript.

REFERENCES

1. **Alon U.** Positive feedback, bistability and memory. In: *An Introduction to Systems Biology*. Boca Raton, FL: CRC Press, 2020, p. 77–96.
2. **Hodgkin AL**, **Huxley AF.** A quantitative description of membrane current and its application to conduction and excitation in nerve. *J Physiol* 117: 500–544, 1952. doi:10.1113/jphysiol.1952.sp004764.
3. **Leloup J-C**, **Goldbeter A.** Modeling the molecular regulatory mechanism of circadian rhythms in *Drosophila*. *BioEssays* 22: 84–93, 2000. doi:10.1002/(SICI)1521-1878(200001)22:1<84::AID-BIES13>3.0.CO;2-I.
4. **Scheper T**, **Klinkenberg D**, **Pennartz C**, **van Pelt J.** A mathematical model for the intracellular circadian rhythm generator. *J Neurosci* 19: 40–47, 1999. doi:10.1523/JNEUROSCI.19-01-00040.1999.
5. **Rorsman P**, **Ashcroft FM.** Pancreatic β-cell electrical activity and insulin secretion: of mice and men. *Physiol Rev* 98: 117–214, 2018. doi:10.1152/physrev.00008.2017.
6. **Cook DL.** Isolated islets of Langerhans have slow oscillations of electrical activity. *Metabolism* 32: 681–685, 1983. doi:10.1016/0026-0495(83)90124-5.
7. **Satin LS**, **Butler PC**, **Ha J**, **Sherman AS.** Pulsatile insulin secretion, impaired glucose tolerance and type 2 diabetes. *Mol Aspects Med* 42: 61–77, 2015. doi:10.1016/j.mam.2015.01.003.
8. **Song SH**, **McIntyre SS**, **Shah H**, **Veldhuis JD**, **Hayes PC**, **Butler PC.** Direct measurement of pulsatile insulin secretion from the portal vein in human subjects. *J Clin Endocrinol Metab* 85: 4491–4499, 2000. doi:10.1210/jcem.85.12.7043.
9. **Nunemaker CS**, **Wasserman DH**, **McGuinness OP**, **Sweet IR**, **Teague JC**, **Satin LS.** Insulin secretion in the conscious mouse is biphasic and pulsatile. *Am J Physiol Endocrinol Metab* 290: E523–E529, 2006. doi:10.1152/ajpendo.00392.2005.
10. **Matveyenko AV**, **Veldhuis JD**, **Butler PC.** Measurement of pulsatile insulin secretion in the rat: direct sampling from the hepatic portal vein. *Am J Physiol Endocrinol Physiol* 295: E569–E574, 2008. doi:10.1152/ajpendo.90335.2008.
11. **Goodner CJ**, **Hom FG**, **Koerker DJ.** Hepatic glucose production oscillates in synchrony with the islet secretory cycle in fasting rhesus monkeys. *Science* 215: 1257–1260, 1982. doi:10.1126/science.7036347.
12. **Matveyenko AV**, **Liuwantara D**, **Gurlo T**, **Kirakossian D**, **Dalla Man C**, **Cobelli C**, **White MF**, **Copps KD**, **Volpi E**, **Fujita S**, **Butler PC.** Pulsatile portal vein insulin delivery enhances hepatic insulin action and signaling. *Diabetes* 61: 2269–2279, 2012. doi:10.2337/db11-1462.
13. **O'Rahilly S**, **Turner RC**, **Matthews DR.** Impaired pulsatile secretion of insulin in relatives of patients with non-insulin-dependent diabetes. *N Engl J Med* 318: 1225–1230, 1988. doi:10.1056/NEJM198805123181902.
14. **Lang DA**, **Matthews DR**, **Burnett M**, **Turner RC.** Brief, irregular oscillations of basal plasma insulin and glucose concentrations in diabetic man. *Diabetes* 30: 435–439, 1981. doi:10.2337/diab.30.5.435.
15. **Kirchgessner AL**, **Pintar JE.** Guinea pig pancreatic ganglia: projections, transmitter content, and the type-specific localization of monoamine oxidase. *J Comp Neurol* 305: 613–631, 1991. doi:10.1002/cne.903050407.
16. **Ushiki T**, **Watanabe S.** Distribution and ultrastructure of the autonomic nerves in the mouse pancreas. *Microsc Res Tech* 37: 399–406, 1997. doi:10.1002/(SICI)1097-0029(19970601)37:5/6<399::AID-JEMT4>3.0.CO;2-9.
17. **King BF**, **Love JA**, **Szurszewski JH.** Intracellular recordings from pancreatic ganglia of the cat. *J Physiol* 419: 379–403, 1989. doi:10.1113/jphysiol.1989.sp017877.
18. **Adablah JE**, **Vinson R**, **Roper MG**, **Bertram R.** Synchronization of pancreatic islets by periodic or non-periodic muscarinic agonist pulse trains. *PLoS One* 14: e0211832, 2019. doi:10.1371/journal.pone.0211832.
19. **Pedersen MG**, **Bertram R**, **Sherman A.** Intra- and inter-islet synchronization of metabolically driven insulin secretion. *Biophys J* 89: 107–119, 2005. doi:10.1529/biophysj.104.055681.
20. **Dhumpa R**, **Truong TM**, **Wang X**, **Bertram R**, **Roper MG.** Negative feedback synchronizes islets of Langerhans. *Biophys J* 106: 2275–2282, 2014. doi:10.1016/j.bpj.2014.04.015.
21. **Roper MG**, **Shackman JG**, **Dahlgren GM**, **Kennedy RT.** Microfluidic chip for continuous monitoring of hormone secretion from live cells using an electrophoresis-based immunoassay. *Anal Chem* 75: 4711–4717, 2003. doi:10.1021/ac0346813.
22. **Yi L**, **Wang X**, **Dhumpa R**, **Schrell AM**, **Mukhitov N**, **Roper MG.** Integrated perfusion and separation systems for entrainment of insulin secretion from islets of Langerhans. *Lab Chip* 15: 823–832, 2015. doi:10.1039/c4lc01360c.
23. **Ferry MS**, **Razinkov IA**, **Hasty J.** Microfluidics for synthetic biology: from design to execution. *Methods Enzymol* 497: 295–372, 2011. doi:10.1016/B978-0-12-385075-1.00014-7.
24. **Angeli D**, **Ferrell JE Jr**, **Sontag ED.** Detection of multistability, bifurcations, and hysteresis in a large class of biological positive-feedback systems. *Proc Natl Acad Sci USA* 101: 1822–1827, 2004. doi:10.1073/pnas.0308265100.
25. **Bertram R**, **Satin LS**, **Zhang M**, **Smolen P**, **Sherman A.** Calcium and glycolysis mediate multiple bursting modes in pancreatic islets. *Biophys J* 87: 3074–3087, 2004. doi:10.1529/biophysj.104.049262.
26. **Yi L**, **Bandak B**, **Wang X**, **Bertram R**, **Roper MG.** Dual detection system for simultaneous measurement of intracellular fluorescent markers and cellular secretion. *Anal Chem* 88: 10368–10373, 2016. doi:10.1021/acs.analchem.6b02404.
27. **Grynkiewicz G**, **Poenie M**, **Tsien R.** A new generation of Ca^{2+} indicators with greatly improved fluorescence properties. *J Biol Chem* 260: 3440–3450, 1985.
28. **Marinelli I**, **Vo T**, **Gerardo-Giorda L**, **Bertram R.** Transitions between bursting modes in the integrated oscillator model for pancreatic β-cells. *J Theor Biol* 454: 310–319, 2018. doi:10.1016/j.jtbi.2018.06.017.
29. **Bertram R**, **Satin LS**, **Sherman AS.** Closing in on the mechanisms of pulsatile insulin secretion. *Diabetes* 67: 351–359, 2018. doi:10.2337/dbi17-0004.
30. **Keizer J**, **Magnus G.** ATP-sensitive potassium channel and bursting in the pancreatic β cell. *Biophys J* 56: 229–242, 1989. doi:10.1016/S0006-3495(89)82669-4.
31. **Denton RM.** Regulation of mitochondrial dehydrogenases by calcium ions. *Biochim Biophys Acta* 1787: 1309–1316, 2009. doi:10.1016/j.bbabio.2009.01.005.
32. **Marinelli I**, **Parekh V**, **Fletcher P**, **Thompson B**, **Ren J**, **Tang X**, **Saunders TL**, **Ha J**, **Sherman A**, **Bertram R**, **Satin LS.** Slow oscillations persist in pancreatic beta cells lacking phosphofructokinase M. *Biophys J* 121: 692–704, 2022. doi:10.1016/j.bpj.2022.01.027.
33. **Marinelli I**, **Fletcher P**, **Sherman AS**, **Satin LS**, **Bertram R.** Symbiosis of electrical and metabolic oscillations in pancreatic β-cells. *Front Physiol* 12: 781581, 2021. doi:10.3389/fphys.2021.781581.
34. **Šterk M**, **Dolenšek J**, **Bombek LK**, **Markovič R**, **Zakelšek D**, **Perc M**, **Pohorec V**, **Stožer A**, **Gosak M.** Assessing the origin and velocity of Ca^{2+} waves in three-dimensional tissue: Insights from a mathematical model and confocal imaging in mouse pancreas tissue slices. *Commun Nonlinear Sci Numer Simul* 93: 105495, 2021. doi:10.1016/j.cnsns.2020.105495.
35. **Benninger RKP**, **Hodson DJ.** New understanding of β-cell heterogeneity and in situ islet function. *Diabetes* 67: 537–547, 2018. doi:10.2337/dbi17-0040.
36. **Benninger RKP**, **Hutchens T**, **Head WS**, **McCaughey MJ**, **Zhang M**, **Le Marchand SJ**, **Satin LS**, **Piston DW.** Intrinsic islet heterogeneity and gap junction coupling determine spatiotemporal Ca^{2+} wave dynamics. *Biophys J* 107: 2723–2733, 2014. doi:10.1016/j.bpj.2014.10.048.
37. **Benninger RKP**, **Zhang M**, **Head WS**, **Satin LS**, **Piston DW.** Gap junctional coupling and calcium waves in the pancreatic islet. *Biophys J* 95: 5048–5061, 2008. doi:10.1529/biophysj.108.140863.
38. **Westacott MJ**, **Ludin NWF**, **Benninger RKP.** Spatially organized β-cell subpopulations control electrical dynamics across islets of Langerhans. *Biophys J* 113: 1093–1108, 2017. doi:10.1016/j.bpj.2017.07.021.
39. **Pørksen N**, **Nyholm B**, **Veldhuis JD**, **Butler PC**, **Schmitz O.** In humans at least 75% of insulin secretion arises from punctuated insulin secretory bursts. *Am J Physiol Endocrinol Physiol* 273: E908–E914, 1997. doi:10.1152/ajpendo.1997.273.5.E908.
40. **Ionescu-Tirgoviste C**, **Gagniuc PA**, **Gubceac E**, **Mardare L**, **Popescu I**, **Dima S**, **Militaru M.** The 3D map of the islet routes throughout the healthy human pancreas. *Sci Rep* 5: 14634, 2015. doi:10.1038/srep14634.

41. **Stagner JI**, **Samols E.** Role of intrapancreatic ganglia in regulation of periodic insular secretions. *Am J Physiol Endocrinol Physiol* 248: E522–E530, 1985. doi:10.1152/ajpendo.1985.248.5.E522.
42. **Pomerening JR**, **Sontag ED**, **Ferrell JE Jr.** Building a cell cycle oscillator: hysteresis and bistability in the activation of Cdc2. *Nat Cell Biol* 5: 346–351, 2003. doi:10.1038/ncb954.
43. **Wang Y-C**, **Ferguson EL.** Spatial bistability of Dpp-receptor interactions during Drosophila dorsal-ventral patterning. *Nature* 434: 229–234, 2005. doi:10.1038/nature03318.
44. **Santillán M**, **Mackey MC**, **Zeron ES.** Origin of bistability in the *lac* operon. *Biophys J* 92: 3830–3842, 2007. doi:10.1529/biophysj.106.101717.
45. **Podobnik B**, **Korošak D**, **Klemen MS**, **Stožer A**, **Dolenšek J**, **Rupnik MS**, **Ivanov PC**, **Holme P**, **Jusup M.** Cells operate collectively to help maintain glucose homeostasi. *Biophys J* 118: 2588–2595, 2020. doi:10.1016/j.bpj.2020.04.005.
46. **Gardner TS**, **Cantor CR**, **Collins JJ.** Construction of a genetic toggle switch in *Escherichia coli*. *Nature* 403: 339–342, 2000. doi:10.1038/35002131.
47. **Beauvois MC**, **Merezak C**, **Jonas J-C**, **Ravier MA**, **Henquin J-C**, **Gilon P.** Glucose-induced mixed $[Ca^{2+}]_c$ oscillations in mouse beta-cells are controlled by the membrane potential and the SERCA3 Ca^{2+}-ATPase of the endoplasmic reticulum. *Am J Physiol Cell Physiol* 290: C1503–C1511, 2006. doi:10.1152/ajpcell.00400.2005.
48. **Zhang M**, **Goforth P**, **Bertram R**, **Sherman A**, **Satin LS.** The Ca^{2+} dynamics of isolated mouse β-cells and islets: implications for mathematical models. *Biophys J* 84: 2852–2870, 2003. doi:10.1016/S0006-3495(03)70014-9.
49. **Bertram R**, **Sherman A**, **Satin LS.** Metabolic and electrical oscillations: partners in controlling pulsatile insulin secretion. *Am J Physiol Endocrinol Physiol* 293: E890–E900, 2007. doi:10.1152/ajpendo.00359.2007.
50. **Bozem M**, **Henquin J-C.** Glucose modulation of spike activity independently from changes in slow waves of membrane potential in mouse B-cells. *Pflugers Arch* 413: 147–152, 1988. doi:10.1007/BF00582524.
51. **Nunemaker CS**, **Zhang M**, **Wasserman DH**, **McGuinness OP**, **Powers AC**, **Bertram R**, **Sherman A**, **Satin LS.** Individual mice can be distinguished by the period of their islet calcium oscillations. *Diabetes* 54: 3517–3522, 2005. doi:10.2337/diabetes.54.12.3517.